JOURNAL OF CATALYSIS 146, 511–522 (1994)

N_2O Reduction by CO over an Alumina-Supported Pt Catalyst: Steady-State Multiplicity

Ramakant R. Sadhankar, Jing Ye, and David T. Lynch[1]

Department of Chemical Engineering, University of Alberta, Edmonton, Alberta, Canada T6G 2G6

Received June 15, 1993; revised October 12, 1993

Steady-State multiplicity of the N_2O + CO reaction over an alumina supported platinum catalyst has been observed over the temperature range 461–520 K. The boundaries of the steady-state multiplicity region have been mapped on a N_2O–CO feed composition diagram, and the effect of temperature on multiplicity was determined. Four kinetic models have been examined, and it was found that only a model based on carbon monoxide self-exclusion from the platinum catalyst was able to describe all of the observed behavior. The CO self-exclusion effect requires that an adsorbed CO molecule exclude other CO molecules from an area equivalent in size to N_{CO} surface Pt atoms, where N_{CO} is slightly greater than unity. The proposed mechanism consists of several elementary steps, namely, the reversible adsorption of CO, the irreversible dissociative adsorption of N_2O to form adsorbed atomic oxygen and gaseous N_2, and the reaction of adsorbed carbon monoxide and atomic oxygen to form gaseous CO_2. Due to the CO self-exclusion effect, N_2O can still adsorb on a Pt surface saturated with CO and therefore the model predicts CO conversions as high as the experimental values for high concentrations of CO in the feed, something which is not possible with the other three mechanisms which were examined. For this model, the steady-state multiplicity can be described by an explicit rate function. © 1994 Academic Press, Inc.

INTRODUCTION

The reduction reactions of the various nitrogen oxides by carbon monoxide over noble metal catalysts have been studied extensively because of their importance in automobile catalytic converters. At a typical exhaust gas temperature of 770 K, while nitric oxide (NO) is present in significant amounts, nitrous oxide (N_2O) is not commonly observed. Therefore, the reduction of NO by CO over noble metal catalysts has been the main focus of several studies. It has been shown that the reduction reaction of NO by CO can exhibit complex behavior such as steady-state multiplicity (1, 2) and self-sustained oscillations (2–8). A catalyst surface reconstruction process for Pt(100) has been suggested (5–7) as possibly being responsible for some of the observed complex behavior. While the exact mechanism by which NO is reduced by CO over supported noble metal catalysts has not been completely determined, several studies (9–18) have reported the formation of N_2O as an intermediate in the overall NO + CO reaction, particularly at temperatures below 580 K. Thus, an understanding of the detailed mechanism of the N_2O + CO reaction is necessary in order to understand the complex behavior of the overall NO + CO reaction over supported noble metal catalysts.

Despite the frequent observation of N_2O formation and reaction during the reduction of NO by CO, the reaction of N_2O with CO on noble metal catalysts has only rarely been the primary focus of an investigation (17, 19–21). Adlhoch *et al.* (19) found that the rate of the N_2O + CO reaction over polycrystalline platinum is two orders of magnitude lower than the rate of the NO + CO reaction, and that N_2O decomposition is the rate-limiting step. Lintz (20) compared the reaction probabilities of the NO + CO, N_2O + CO, and O_2 + CO reactions over polycrystalline platinum and proposed an elementary reaction sequence for the N_2O + CO reaction. McCabe and Wong (17) investigated the kinetics of the N_2O + CO reaction over a supported rhodium catalyst and proposed a mechanism for the reaction. They also reported that the N_2O + CO reaction rate is several orders of magnitude lower than the rates of the NO + CO and O_2 + CO reactions. Cho (21) presented a kinetic analysis showing that the rate of the N_2O + CO reaction, as an intermediate reaction in the NO + CO reaction system, can be two to three orders of magnitude higher than the rate of the isolated N_2O + CO reaction.

It is possible that the lack of a single rate-controlling step for all conditions is responsible for the several different mechanisms having been proposed for the reduction reaction of N_2O by CO. Alternatively, the fact that a derived rate expression is consistent with the experimental data provides only a necessary but not a sufficient condition that a model is based upon the correct reaction

[1] To whom correspondence should be addressed.

0021-9517/94 $6.00

mechanism. Very good agreement is often possible solely because rate functions of the Langmuir–Hinshelwood type are very adept at fitting data. An additional interesting observation is that, despite the similarity of the N_2O + CO and O_2 + CO reaction systems, there are as yet no reports in the literature of multiplicity behavior for the N_2O + CO reaction on noble metal catalysts.

In an earlier study, Graham and Lynch (22), used the steady-state multiplicity behavior of the O_2 + CO reaction over a supported platinum catalyst to discriminate among several kinetic models. In this study, a similar discrimination among several kinetic models will be performed by using the experimental bifurcation behavior for the reduction of N_2O by CO over a supported platinum catalyst. Only a model incorporating a CO self-exclusion effect is found to be able to describe the experimental data.

METHODS

The recycle reactor system used in this study has been previously described by Lynch and Wanke (23). The subsequent modifications to the feed metering and controlling system have been described by Graham and Lynch (22, 24). Further modifications to the equipment including gas analyzers and computer automation are described herein.

The recycle reactor contained 20 g of Englehard catalyst containing 0.5 wt% platinum supported on γ-Al_2O_3 in the form of pellets. The cylindrical pellets were approximately 3 mm by 3 mm in size, with the Pt deposited in a thin layer on the exterior portion of the pellets. From an earlier investigation (24) on a different batch of the same type of catalyst, the total surface area of the platinum catalyst, a, is estimated to be 9.4 m^2 and the adsorption capacity of the platinum catalyst, L, is assumed to be 2×10^{-5} mol/m^2 of platinum surface. The catalyst bed was diluted with 60 g of 3-mm-diameter glass beads. As a result of some of the modifications to the recycle tubing, the effective free volume of the recycle system including the reactor (without the catalyst and the glass beads), metal bellows compressor and associated tubing was determined to be 215 cm^3 from frequency response measurements similar to those described by Lynch and Walters (25). The reactor pressure was always maintained at 103 kPa and the temperatures used in this study were 461, 480, 499, and 520 K. The recycle flow from the pump was measured to be 500 cm^3/s. Thus, for a feed flow rate of 185 cm^3 (STP)/min, a recycle ratio of 85 to 98 was achieved at the reactor operating conditions. From frequency response measurements, the mixing in the reactor was found to approximate closely that of an ideal CSTR.

The flow controllers and valves for controlling the feed composition were interfaced to an IBM-compatible personal computer using Optomux digital/analogue conversion equipment. This equipment was also used for monitoring reactor temperatures and individual and total flow rates. The gases used for this study were purchased from Linde and included gas mixtures of 2, 5, or 10% CO in N_2; 2 or 10% N_2O in N_2; and prepurified N_2. Feed compositions were in the ranges of 0–2% N_2O and 0–2% CO, with nitrogen for the balance of the feed.

The effluent stream from the recycle reactor was routed through two infrared-type gas analyzers connected in series. Horiba infrared gas analyzers model PIR-2000 and VIA-300 were used for measuring CO_2 and N_2O concentrations, respectively. The analyzers were calibrated at the beginning of each experiment, using N_2 for zero calibration and a gas mixture (0.982% CO_2 in N_2, 2% CO_2 in N_2, or 2% N_2O in N_2) for span calibration.

RESULTS

The experiments were concerned with examining the reaction rate dependence on concentration, and the steady-state multiplicity behavior, in the temperature range 460–520 K. Matsuura and Kato (26) have shown that steady-state rate multiplicity occurs for heterogeneous catalytic reactions in an isothermal CSTR when the reactant concentration in the feed is such that the rate curve intersects the CSTR mass balance line at three points on a rate versus reactant concentration plot. At least one of the three steady states is always unstable when multiplicity occurs. This type of feed concentration multiplicity can occur even in the absence of intrinsic rate multiplicity which can be represented by hysteresis in the rate versus reactor concentration curve. Eigenberger (27) has shown that intrinsic rate multiplicity can be caused by the competing chemisorption of two species upon the same active sites of a catalyst and that the rate expression has to be implicit to possess multiple solutions. The experiments described herein were aimed at studying multiplicity of the type described by Matsuura and Kato (26) rather than intrinsic rate multiplicity as described by Eigenberger (27). Emphasis was particularly placed on determination of the reactor feed composition at which bifurcation in steady-state CO conversion occurs. The term "bifurcation point" will be used to refer to the CO feed concentration at which the CO conversion changes from a low to a high value, or from a high to a low value.

In the first group of experiments, the reactor temperature, the total feed flow rate to the reactor and the N_2O concentration in the feed were held constant while varying the CO feed concentration during each experimental run. Sets of measurements were made at each of three different temperatures, 461, 480, and 499 K, respectively, and at each temperature experiments were carried out using three different feed N_2O concentrations, 0.4, 0.7, and 1.2%, respectively. The results of these nine sets of experimental data are summarized in Fig. 1.

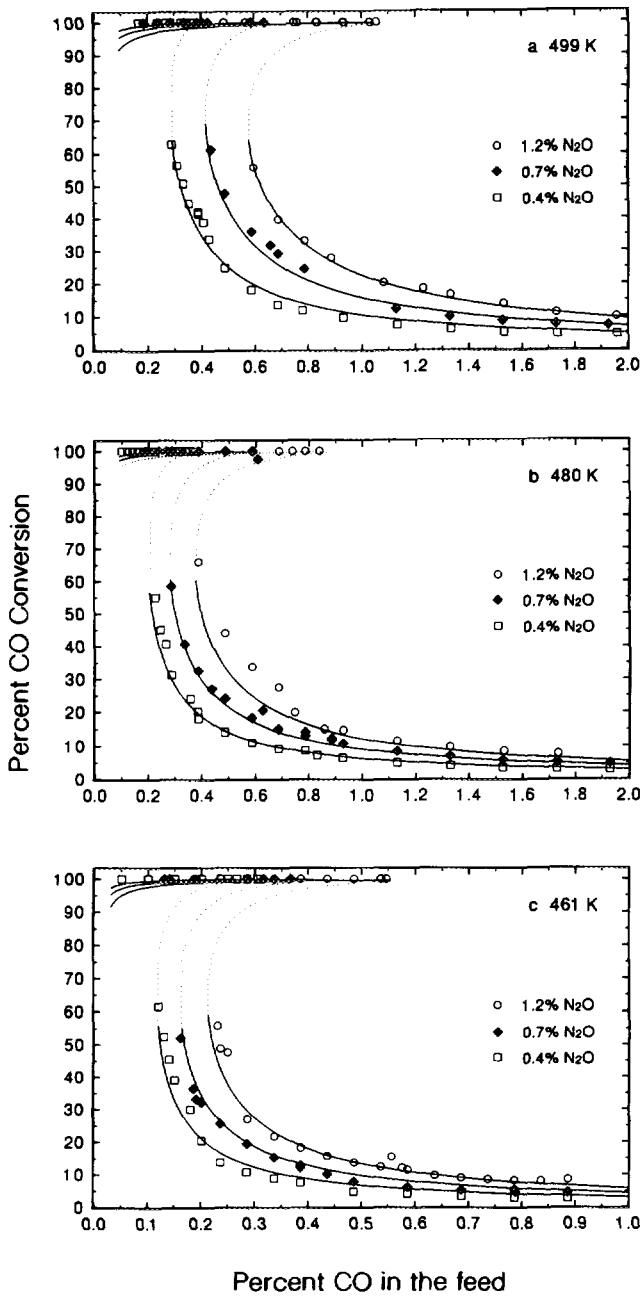

FIG. 1. Multiplicity behavior during the reduction of N_2O by CO at 461–499 K: (———) predictions from Mechanism 4; (---) unstable steady states predicted by Mechanism 4.

At the beginning of each experiment, the CO feed concentration was set to be much less than the N_2O feed concentration. The attainment of steady-state was determined by monitoring the CO_2 and N_2O concentrations in the reactor effluent stream. The CO feed concentration was then increased in steps, allowing a minimum of 3 h at every step to reach steady-state conditions. It was observed that, while the CO conversion was 100% at low CO feed concentrations, increasing the CO concentration beyond a certain limit (high-to-low conversion bifurcation point) caused the CO conversion to drop from nearly 100% to a very low value. For example, for the rightmost curve in Fig. 1a (499 K, 1.2% N_2O), the high-to-low conversion bifurcation occurred for a feed containing between 1.055 and 1.082% CO. Each experiment was then repeated starting with a feed CO concentration which was much in excess of the feed N_2O concentration (low CO conversion region). Stepwise decreases of the %CO in the feed caused the conversion to increase gradually (from nearly 10% at 1.96% CO to nearly 55% at 0.596% CO, as shown by the open circles in Fig. 1a). Further decreases in CO feed concentration, below the low-to-high conversion bifurcation point, caused the CO conversion to increase to 100%. In Fig. 1a, the low-to-high conversion bifurcation occurred at a feed CO composition of between 0.586% and 0.596% for the experiment with 1.2% N_2O in the feed. The bifurcation points were bracketed by repeating the experiments with small step sizes in CO feed concentration, until reproducible steady-states were achieved. Operating periods of much longer than 3 h were often necessary in order to bracket a bifurcation point.

An additional three sets of experiments were carried out at 520 K by reversing the roles of CO and N_2O. For the experiments at 520 K, the N_2O concentration in the feed was varied while holding the %CO in the feed constant for each of the experimental runs. The results of three runs, with feed CO of 0.676, 0.915, and 1.166%, respectively, are summarized in Fig. 2. Although Fig. 2 has a totally different appearance when compared to Figs. 1a–1c, the multiplicity behavior shown in both of the figures is similar. As can be seen from Fig. 2, almost 100% CO conversion was obtained for experiments with N_2O in large excess relative to

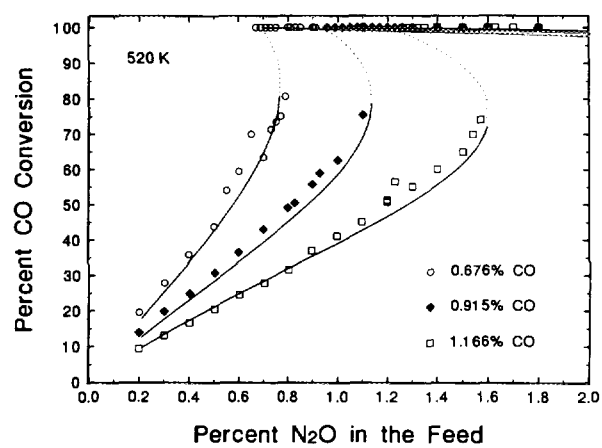

FIG. 2. Multiplicity behavior during the reduction of N_2O by CO at 520 K: (———) predictions from Mechanism 4; (---) unstable steady states predicted by Mechanism 4.

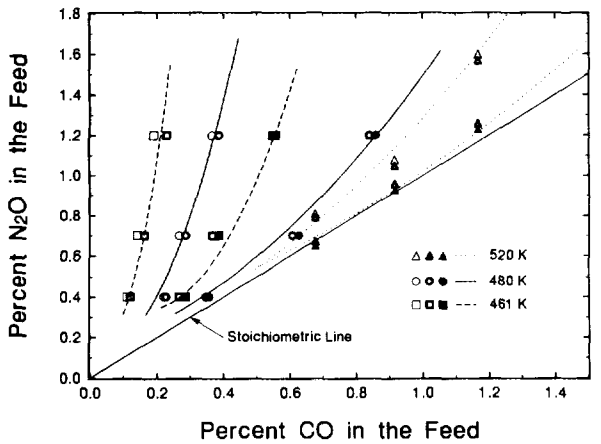

FIG. 3. Dependence of bifurcation points on temperature and feed composition: (—, – – –, ...) predictions from Mechanism 4.

CO. Decreasing the N_2O concentration below the composition corresponding to the high-to-low conversion bifurcation point caused the CO conversion to drop from 100% to a much lower value. A low CO conversion was obtained in the experiments which were started with excess CO in the feed. Increasing the N_2O in the feed led to a gradual increase in the CO conversion. Near the low-to-high conversion bifurcation point, the CO conversion increased rapidly to 100%.

The experimental locations of the bifurcation points are shown by paired sets of symbols in Fig. 3. The pair of an empty symbol and a half-filled symbol brackets a low-to-high conversion bifurcation point and the pair of a half-filled symbol and a filled symbol brackets a high-to-low conversion bifurcation point. The bifurcation points at 499 K are not shown in Fig. 3 for reasons of clarity. The low-to-high conversion bifurcation points at 499 K almost coincide with the high-to-low conversion bifurcation points at 461 K. The high-to-low conversion bifurcation points at 499 K lie between the two 520 K bifurcation boundaries. The multiplicity region lies within the two bifurcation boundaries. In the region to the left of the low-to-high conversion bifurcation boundary, CO conversion is almost 100%. The low conversion region lies to the right of the high-to-low conversion bifurcation boundary. It can be seen from Fig. 3 that the bifurcation point locations shift in the direction of higher %CO with increasing temperature and increasing $\%N_2O$ in the feed.

It is generally agreed that during N_2O reduction by CO, an adsorbed oxygen species is formed through N_2O decomposition. In addition to reaction with CO, it is possible that an oxygen desorption reaction could also be involved as a process for removal of surface oxygen. Therefore, a sensitive oxygen analyzer (Customs Sensors and Technology Model 8205, lowest range 0–2 ppm O_2) was employed to measure reactor oxygen content with a feed consisting of 1.5% N_2O in N_2 at 499 K. No change in oxygen content between the feed and the effluent streams could be detected, therefore, oxygen desorption does not occur in the temperature range under consideration. In another experiment with a feed containing 2% CO in N_2, no CO_2 could be detected in the reactor effluent, therefore reaction between two adsorbed CO molecules to form CO_2 and surface carbon does not occur at the temperatures used in this study.

To ensure that the experimental measurements represent the intrinsic kinetics of the reaction, it is necessary to determine to what extent, if any, the experimental observations have been affected by internal and external mass transfer limitations. The absence of interparticle mass transfer effects was verified experimentally by varying the recycle flow delivered by the pump. No effect on the CO conversion was observed for a wide range of recycle flow rates. In addition, the ratio of the surface CO concentration to bulk CO concentration, calculated from a mass transfer coefficient correlation (28), was predicted to be approximately 0.995 for the experiments, which further confirms the absence of interparticle mass transfer resistance. The intraparticle diffusional effects were expected to be negligible because the catalyst was an egg-shell-type catalyst in which all of the platinum was deposited in the outer 10% (or less) of the volume of the pellets. Moreover, the per-pass conversion in the reactor was always less than 1%.

Intraparticle diffusional effects were also assessed by determining the value of a Thiele modulus of the form

$$\Phi_S = \frac{r_p^2(-R_{CO})}{D_{eff}C_S}. \qquad [1]$$

Satterfield (28) suggests that, for an isothermal system consisting of an irreversible reaction of a single reactant, whose kinetics can be represented by a power-law relationship, intrinsic kinetics are observed if $\Phi_S < 6$ for a zeroth-order reaction or $\Phi_S < 1$ for a first-order reaction. In addition, Smith *et al.* (29) have shown that for a negative-order reaction, $\Phi_S < 10$ is sufficient for intrinsic kinetics to be measured. For the experimental data in the low-conversion regions of Figs. 1 and 2 (negative-order kinetics with respect to CO), the calculated values of Φ_S vary from a low of 0.01 (at 461 K for 0.4% N_2O and 0.88% CO in the feed) to a high of 1.6 (at 520 K with 0.8% N_2O and 0.67% CO in the feed). Therefore, it can be said that the measurements in the low-conversion region are not affected by internal diffusion limitations. Unfortunately, the same cannot be stated conclusively for the high-conversion region (positive-order kinetics with almost 100% CO conversion) because it was not possible to determine

the very low reactor concentrations reliably with the gas analysis equipment employed in this study. Thus, because of the possibility of diffusional effects on the high-conversion data, emphasis has been placed in the following on using the low-conversion data for discriminating among the various mechanisms and for estimating the model parameters. The high-conversion data has only been used to the extent that, when estimating parameters, an attempt has always been made to have model-experimental agreement regarding the locations of the high-to-low conversion bifurcation points.

DISCUSSION

The overall reaction in which CO is oxidized by N_2O involves elementary steps consisting of adsorption, desorption, and surface reaction. In the temperature range of interest (<600 K), CO adsorbs reversibly on platinum (30). The adsorption and/or decomposition of N_2O on platinum and other noble metal catalysts have been studied by several authors. Lintz and Riekert (31) compared the reaction probabilities of N_2O decomposition from several studies and they concluded that the observations regarding the N_2O/Pt system were quite reproducible. Alnot *et al.* (32) reported the dissociative adsorption of N_2O on a recrystallized platinum ribbon with the release of molecular N_2 in the temperature range 300–500 K. Takoudis and Schmidt (33) studied the kinetics of N_2O decomposition on polycrystalline Pt in the temperature range of 673–1473 K and proposed a Langmuir–Hinshelwood rate expression. In their derivation, the rate-limiting step was assumed to be the decomposition of adsorbed N_2O, while adsorption–desorption equilibrium was assumed for both N_2O and O_2. They also concluded that the surface coverage of adsorbed N_2O is equal to unity at low temperature and proportional to the partial pressure of N_2O at high temperatures. However, in a later study, Schmidt *et al.* (34) reported that N_2O does not appear to chemisorb on platinum in UHV experiments in the temperature range 700–1600 K.

The surface reaction between adsorbed CO and adsorbed oxygen is believed to be the main reaction for the production of CO_2 (17, 21) when CO is oxidized by N_2O. However, an Eley–Rideal-type reaction between gas-phase CO and adsorbed oxygen has also been suggested (20) as a route for the production of CO_2 in the overall N_2O + CO reaction.

A main consideration in proposing a reaction mechanism is that it should be able to describe the experimental multiplicity behavior. In this study, four mechanisms have been examined in an attempt to describe the experimental bifurcation and reaction rate behavior of the N_2O + CO reaction.

Mechanism 1

The first mechanism used to describe the rate multiplicity was a classical Langmuir–Hinshelwood-type model consisting of the following elementary steps:

$$\mathrm{CO(g)} + M \rightleftharpoons \mathrm{CO}\text{–}M \quad [2]$$

$$\mathrm{N_2O(g)} + M \rightarrow \mathrm{N_2(g)} + \mathrm{O\text{–}M} \quad [3]$$

$$\mathrm{CO\text{–}M} + \mathrm{O}\text{–}M \rightarrow \mathrm{CO_2(g)} + 2M. \quad [4]$$

At steady state, the mass balance equations for the adsorbed species can be written as follows, where all parameters are defined in the Notation Appendix:

$$k_1L[\mathrm{CO}](1 - \theta_{\mathrm{CO}} - \theta_{\mathrm{O}}) - k_{-1}L\theta_{\mathrm{CO}} - k_3L^2\theta_{\mathrm{O}}\theta_{\mathrm{CO}} = 0 \quad [5]$$

$$k_2L[\mathrm{N_2O}](1 - \theta_{\mathrm{CO}} - \theta_{\mathrm{O}}) - k_3L^2\theta_{\mathrm{O}}\theta_{\mathrm{CO}} = 0. \quad [6]$$

Equations [5] and [6] can be solved to express the fractional surface coverage of CO and oxygen in terms of the CO and N_2O gas-phase concentrations as given by

$$\theta_{\mathrm{CO}} = \frac{K_1[\mathrm{CO}] - (K_{21} + K_{23})[\mathrm{N_2O}]}{1 + K_1[\mathrm{CO}] - K_{21}[\mathrm{N_2O}]} \quad [7]$$

$$\theta_{\mathrm{O}} = \frac{K_{23}[\mathrm{N_2O}]}{K_1[\mathrm{CO}] - K_{21}[\mathrm{N_2O}]}, \quad [8]$$

respectively. The specific rate of CO_2 formation is given by

$$\mathbf{r}_{\mathrm{CO_2}} = K_{\mathrm{LH}}\theta_{\mathrm{O}}\theta_{\mathrm{CO}}. \quad [9]$$

The reactor is assumed to be an ideal CSTR, and therefore, the gas-phase species mass balances are given by the following two equations:

$$Q([\mathrm{CO}]_0 - [\mathrm{CO}]) = WK_{\mathrm{LH}}\theta_{\mathrm{O}}\theta_{\mathrm{CO}} \quad [10]$$

$$Q([\mathrm{CO}]_0 - [\mathrm{CO}]) = Q([\mathrm{N_2O}]_0 - [\mathrm{N_2O}]). \quad [11]$$

Equations [7], [8], [10], and [11] can be used to relate the percentage CO conversion to the reactant compositions in the reactor. Because the experimental CO conversion is known as a function of reactant concentrations, it is possible to estimate the values of the kinetic parameters so as to obtain agreement between the model and the data. An initial estimate of the parameters was obtained by forcing the model predictions to match the low-to-high conversion bifurcation point locations. The experimental data for near 100% CO conversion were not used for the initial parameter estimation, because it was not possible to determine the very low reactor concentrations reliably with the gas analysis equipment employed in this study

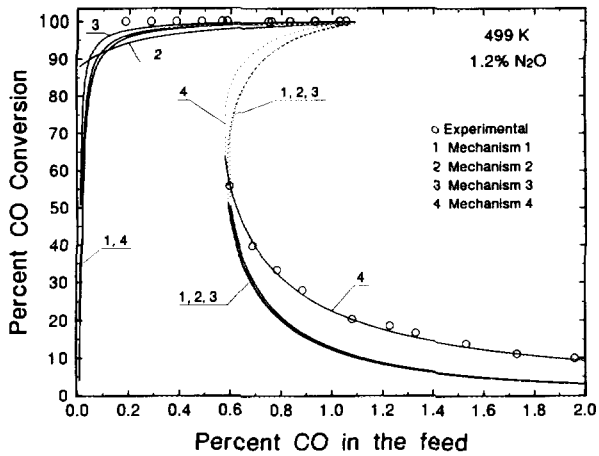

FIG. 4. Comparison of predictions from Mechanisms 1–4 to experimental bifurcation point locations and CO conversions.

when the CO conversion approached 100%. The final parameter values were selected to minimize the sum of squared errors in the predicted bifurcation points.

In Fig. 4, the CO conversion predictions from Mechanism 1 are compared with the experimental data (represented by the open circles) at 499 K with 1.2% N_2O in the feed. The parameter values used for Fig. 4 are listed in Table 1. To generate a continuous curve, Equations [7], [8], [10], and [11] were reduced to a single, cubic equation in $[N_2O]$ by successive substitution. The roots of the cubic equation for $[N_2O]$ were then determined by the "roots" function of MATLAB (35) with different values of the %CO in the feed. The $[N_2O]$ equation has three physically reasonable roots in the region of multiplicity. The dotted lines in Fig. 4 indicate that the steady state is unstable; in the multiplicity region two of the steady states are stable and one is unstable. It can be seen from Fig. 4 that the predictions from Mechanism 1 match the experimental bifurcation points. However, the predicted CO conversions are somewhat less than the experimental values in the region of low feed CO concentrations (<0.3%CO) and very markedly less than the experimental values in the region of high feed CO concentrations (0.6–2%). An attempt was made to adjust the parameter values to obtain better agreement between the experiments and the predictions, however, it was not possible to find a single set of parameter values that could describe both the experimental CO conversions as well as the bifurcation point locations.

It is possible to increase the CO conversion on the high conversion branch (the region of low %CO in the feed) either by increasing the CO adsorption-desorption constant, K_1, or by reducing the values of the parameters K_{21} or K_{23}. However, adjusting the parameters in this fashion leads to an increasing discrepancy between the predicted and the experimental locations of the high-to-low conversion bifurcation points. It is seen in Fig. 4 that the predicted CO conversion decreases rapidly as the CO in the feed is reduced below approximately 0.2%. This occurs because N_2O decomposition is increasingly favored over CO adsorption as the feed %CO is reduced while holding feed $\%N_2O$ constant. Thus, the oxygen surface coverage increases rapidly and inhibits CO adsorption. As the oxygen surface coverage approaches unity, the CO fractional surface coverage, and consequently the CO conversion, decrease to zero. This is at odds with the experimental data in which the CO conversion was observed to be constant at close to 100% as the feed %CO was decreased. It should be noted, however, that reliable experimental measurements were not possible for very low values of the %CO in the feed because of the previously noted analyzer limitations. The problem of oxygen saturating the surface would not occur if oxygen desorption occurs to any significant extent. However, this explanation is not applicable because, as already mentioned, the possibility of oxygen desorption was examined experimentally and ruled out.

The model predictions for the low conversion branch (high feed %CO) could be improved only slightly by increasing K_{LH} or by reducing K_1, but this can only be achieved at the expense of an increasing discrepancy in the prediction of the low-to-high conversion bifurcation point location. Specifically, both of the bifurcation points shift in the direction of higher feed %CO for an increase in K_{LH} or for a decrease in K_1 or K_{23}. Both bifurcation points are relatively insensitive to changes in the value of K_{21} by as much as ±75%.

From the preceding it is seen that the standard Langmuir–Hinshelwood-type model has serious deficiencies. Although, this mechanism can describe the multiplicity behavior, it is not possible for any single set of model

TABLE 1

Parameter Values at 499 K for Mechanisms 1–4

	Mechanism			
Parameter	1	2	3	4
K_1	1000	2115	605	1200
K_{21}	0.019	0.045		0.0173
K_{23}	8	39.4		8
K_{31}			0.00145	
K_{43}		4.9		
K_5			4.8	
K_{63}			2.4	
K_{65}			0.15	
K_{LH}	1.72×10^{-6}	3.89×10^{-7}	1.72×10^{-6}	1.308×10^{-6}
N_{CO}				1.025

parameter values to produce complete agreement with all of the experimental behavior (bifurcation point locations and reaction rate dependence of feed composition).

Mechanism 2

Lintz (20) proposed a mechanism for the N_2O + CO reaction over polycrystalline Pt which, in addition to the three steps of Mechanism 1, also included an Eley–Rideal (ER) reaction between gas-phase CO and adsorbed oxygen:

$$CO(g) + O\text{–}M \rightarrow CO_2(g) + M. \quad [12]$$

Thus, Mechanism 2 consists of the four reaction steps [2]–[4] and [12]. The steady-state balance for the adsorbed CO is identical to Eq. [5], and the balance for the oxygen species is given by

$$k_2L[N_2O](1 - \theta_{CO} - \theta_O) - k_3L^2\theta_O\theta_{CO} - k_4L[CO]\theta_O = 0. \quad [13]$$

The rate of CO_2 formation is given by

$$r_{CO_2} = K_{LH}\theta_O(\theta_{CO} + K_{43}[CO]). \quad [14]$$

Equations [5] and [13] cannot be solved explicitly for the fractional surface coverages of CO and oxygen in that quadratic equations are obtained for θ_{CO} and θ_O. Therefore, Eqs. [5], [10], [11], and [13] were reduced to a single, tenth-order polynomial in $[N_2O]$ and solved by using the MATLAB "roots" function. The $[N_2O]$ polynomial has three physically reasonable roots in the region of multiplicity and a single physically reasonable root elsewhere. As can be seen from Fig. 4, Mechanism 2 predicts near 100% conversion of CO at low %CO in the feed. The model parameter, K_{43}, which is the ratio of the reaction rate constants for the ER and the surface reactions, has a value of 4.9. However, in an extensive review of CO oxidation on noble metal catalysts, Engel and Ertl (30) concluded that for CO oxidation over Pt catalysts there is a lack of evidence for the ER reaction proceeding to any significant degree. Thus, in order to predict high CO conversions in the low feed %CO region, it is necessary to have a very large value for the ER rate constant, relative to the LH rate constant, which is inconsistent with earlier studies. In addition, as seen in Fig. 4, the use of the ER reaction does not produce any improvement in the prediction of the low conversion branch, relative to Mechanism 1. Hence, the inclusion of an ER reaction step cannot be used to eliminate the model–experimental discrepancies noted in Mechanism 1.

Mechanism 3

In the earlier two models, it has been assumed that N_2O adsorbs dissociatively on a platinum surface. However, as suggested by Takoudis and Schmidt (33), N_2O decomposition on platinum could occur via an adsorbed N_2O species as follows:

$$N_2O(g) + M \rightleftharpoons N_2O\text{–}M \quad [15]$$

$$N_2O\text{–}M \rightarrow N_2(g) + O\text{–}M. \quad [16]$$

Mechanism 3 consists of four steps, namely, reactions [2], [4], [15], and [16]. McCabe and Wong (17) used a similar mechanism to describe N_2O reduction by CO on an alumina-supported rhodium catalyst in the temperature range 550 to 700 K. They assumed that a weakly adsorbed N_2O serves as a precursor to dissociative adsorption. The steady-state balances for the three adsorbed species yield the following equations:

$$k_1L[CO](1 - \theta_{CO} - \theta_O - \theta_{N_2O}) - k_{-1}L\theta_{CO} - k_3L^2\theta_O\theta_{CO} = 0 \quad [17]$$

$$k_5L[N_2O](1 - \theta_{CO} - \theta_O - \theta_{N_2O}) - k_{-5}L\theta_{N_2O} - k_6L\theta_{N_2O} = 0 \quad [18]$$

$$k_6L\theta_{N_2O} - k_3L^2\theta_O\theta_{CO} = 0. \quad [19]$$

Equations [17]–[19] can be rearranged to produce explicit expressions for the fractional surface coverages of CO, oxygen and N_2O, namely:

$$\theta_{CO} = \frac{K_1(1 + K_{65})[CO] - K_5K_{63}(1 + K_{31})[N_2O]}{(1 + K_{65})(K_1[CO] + 1) + K_5(1 - K_{31}K_{63})[N_2O]} \quad [20]$$

$$\theta_O = \frac{K_5K_{63}[N_2O]}{(1 + K_{65})K_1[CO] - K_5K_{31}K_{63}[N_2O]} \quad [21]$$

$$\theta_{N_2O} = \frac{\theta_{CO}\theta_O}{K_{63}}. \quad [22]$$

The rate of CO_2 formation is given by Eq. [9]. Unfortunately, as shown in Fig. 4, the CO conversion predictions from Mechanism 3 are very similar to those from Mechanism 1. This was found to occur for all sets of parameter values examined provided that model–experimental agreement concerning the location of the bifurcation points was required. Thus, the existence of an adsorbed N_2O surface species cannot resolve the model–experimental discrepancies noted in Mechanism 1.

Mechanism 4

As shown in the preceding, for feed CO in the range 0.6–2%, all three of the models predict CO conversions

which are much less than the experimental observations. Therefore it can be concluded that the classical Langmuir–Hinshelwood–Hougen–Watson (LHHW)-type mechanisms which were examined cannot describe the overall reaction behavior. In a study of the O_2 + CO reaction, Graham and Lynch (22) encountered similar problems with the classical LHHW mechanisms. They found that, in order to obtain model–experimental agreement, it was necessary to invoke a CO self-exclusion effect, which proposes that an adsorbed CO molecule excludes other CO molecules from an area equivalent to N_{CO} surface Pt atoms, where N_{CO} is slightly larger than unity. The experimental evidence for this effect is provided by the studies of Freel (36), Dorling and Moss (37), and Yao *et al.* (38) who have shown that the fractional saturation coverage of adsorbed CO on small particle size (<5 nm) supported platinum is less than unity. Based on these studies, the CO self-exclusion factor, N_{CO}, has a value in the range of 1.0 to 1.25 corresponding to a CO fractional saturation coverage of 0.8 to 1.0 on a highly dispersed catalyst.

The CO self-exclusion effect does not add any additional steps to a reaction mechanism, instead it modifies the mathematical form of the rate expression for CO adsorption. Graham and Lynch (22) showed that the rate of CO adsorption with the CO self-exclusion effect is given by

$$r_{CO,ads} = k_1 L[CO](1 - \theta_{CO} - \theta_O)\frac{(1 - N_{CO}\theta_{CO})}{(1 - \theta_{CO})}. \quad [23]$$

In a classical Langmuir–Hinshelwood model (e.g., Mechanism 1) $N_{CO} = 1$ which results in Eq. (23) becoming identical to the CO-adsorption term used in Eq. [5]. Mechanism 4 consists of the same elementary steps as Mechanism 1, except that the CO self-exclusion effect has been added. For reactions [2]–[4] the steady-state balance for adsorbed oxygen is given by Eq. [6]. However, due to the CO self-exclusion effect, the steady-state balance for adsorbed CO is modified to become

$$k_1 L[CO](1 - \theta_{CO} - \theta_O)\frac{(1 - N_{CO}\theta_{CO})}{(1 - \theta_{CO})} - k_{-1}L\theta_{CO} - k_3 L^2\theta_{CO}\theta_O = 0. \quad [24]$$

Equations [6] and [24] can be solved explicitly for θ_{CO} and θ_O, yielding

$$\theta_{CO} = \frac{K_1[CO] - (K_{21} + K_{23})[N_2O]}{1 + N_{CO}K_1[CO] - K_{21}[N_2O]} \quad [25]$$

$$\theta_O = \frac{K_{23}[N_2O](1 + (N_{CO} - 1)K_1[CO] + K_{23}[N_2O])}{(K_1[CO] - K_{21}[N_2O]) + K_{23}[N_2O](N_{CO}K_1[CO] - K_{21}[N_2O])}. \quad [26]$$

It is seen that Eqs. [25] and [26] reduce to Eqs. [7] and [8], respectively, for a value of N_{CO} equal to unity. The rate of formation of CO_2 is given by Eq. [9]. It can be seen from Fig. 4 that the predictions from Mechanism 4 are markedly improved relative to the first three mechanisms. The CO conversion predictions for the low-conversion branch exactly match the experimental results while maintaining agreement with the location of the bifurcation points, something which was not possible for the first three mechanisms. Because of the CO self-exclusion effect, N_2O can still adsorb on a surface saturated with CO and, therefore, the predicted CO conversions are as high as the experimental values. Of course, the CO self-exclusion effect does not significantly affect the conversion predictions in the high-conversion region because in this region the CO fractional surface coverage is very low.

A further test for Mechanism 4 is to determine if the predictive ability of the model is not limited to just the data in Fig. 4, but instead can be used over a wide range of experimental conditions. As shown in Figs. 1 and 2, for a constant value of the CO self-exclusion factor, $N_{CO} = 1.025$, the conversion predictions of Mechanism 4 are in excellent agreement with the twelve sets of experimental data which span wide ranges of temperature and feed compositions. In addition, as shown in Fig. 3, Mechanism 4 is also able to describe the composition and temperature dependence of the bifurcation boundaries.

As given in Table 2, different sets of values for the rate parameters (K_1, K_{21}, K_{23}, K_{LH}) are, of course, needed for each of the four different temperatures used in the experiments. However, from Fig. 5 it is seen that an Arrhenius-type temperature dependency holds for each of the four rate parameters. It should be noted that, because several of the rate parameters are ratios of rate constants, it is possible to have both positive and negative slopes. Thus, except for K_{LH}, the values of E/R given in Table 2 are grouped terms which are not true activation energies. Assuming that CO adsorption is nonactivated, the activation energy for CO desorption, E_{-1}, is calculated from E_1/R to be 41.0 kJ/mol. Similarly, the activation energy of the surface reaction between adsorbed CO and adsorbed oxygen, E_3, is calculated from E_{LH}/R to be 74.5 kJ/mol. The activation energy for the N_2O dissociation reaction, E_2, can be calculated from either the sum of E_{23}/R and E_{LH}/R or by subtracting E_1/R from E_{21}/R. The former approach yields a value of 91.2 kJ/mol while the latter gives a value of 92.7 kJ/mol. It is seen that both approaches give similar results, with the average value of E_2 being 92 kJ/mol.

The above values of activation energies obtained from estimating the parameters for Mechanism 4 can be compared with values obtained from other studies. Mechanism 4 predicts that the CO fractional surface coverage is close to its saturation value of $1/N_{CO}$ in the region of

TABLE 2

Temperature Dependence of Parameters for Mechanism 4

Parameter	461 K	480 K	499 K	520 K	E/R
K_1	2550	1725	1200	750	-4931 ($=E_1/R$)
K_{21}	0.0063	0.0106	0.0173	0.0291	6215 ($=E_{21}/R$)
K_{23}	5.4	6.6	8.0	8.8	2029 ($=E_{23}/R$)
K_{LH}	3.30×10^{-7}	7.16×10^{-7}	13.08×10^{-7}	31.0×10^{-7}	8951 ($=E_{LH}/R$)
N_{CO}	1.025	1.025	1.025	1.025	

high %CO in the feed (the low conversion region) and drops sharply to a very low value ($\theta_{CO} < 0.1$) when the feed %CO is decreased below the low-to-high bifurcation point (the high conversion region). The apparently low value (41 kJ/mol) of the CO desorption activation energy, E_{-1}, which is needed to describe the experimental data can be attributed to the existence of a CO saturated surface when the CO conversion is low. Ertl *et al.* (39), using a combination of TPD, LEED, and work function measurements, reported that the activation energy of adsorption of CO on Pt(111) declined with CO surface coverage. They reported that the activation energy of adsorption decreases linearly from 138 kJ/mol at $\theta_{CO} \approx 0$ to 113 kJ/mol at $\theta_{CO} = 0.5$, at which point a sharp decrease to 92 kJ/mol occurred, followed by a rapid decrease in E_{-1} for $\theta_{CO} > 0.6$. They derived an isosteric heat of adsorption of approximately 54 kJ/mol at $\theta_{CO} = 0.7$ from LEED data. Seebauer *et al.* (40) also reported a similar coverage dependence for the heat of adsorption of CO on Pt(111) using laser-induced thermal desorption measurements. They found that the heat of adsorption of 134 kJ/mol at low coverage declined rapidly with surface coverage to a low value of 42 kJ/mol at near saturation coverage of $\theta_{CO} > 0.6$. The preexponential factor for CO desorption was also reported to have a low value of 3×10^7 for a CO saturated surface. The value of E_{-1} of 41.0 kJ/mol used in this study to describe the experimental data is thus seen to be very close to the values of 54 and 42 kJ/mol reported by Ertl *et al.* (39) and Seebauer *et al.* (40), respectively, for a CO saturated Pt(111) surface.

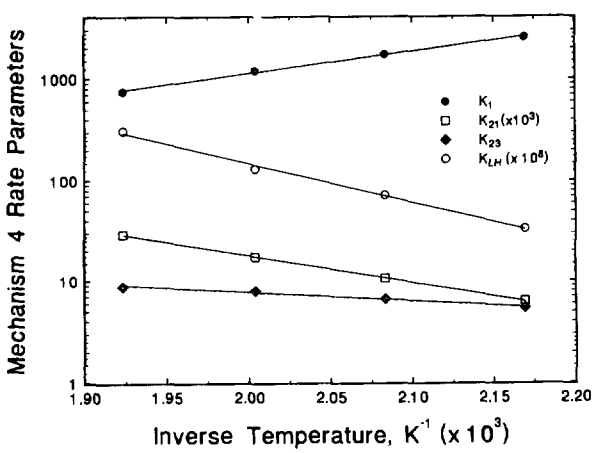

FIG. 5. Arrhenius-type plot of parameters for Mechanism 4.

In an extensive review of CO oxidation over platinum, Engel and Ertl (30) reported that the value of the activation energy of the LH reaction between adsorbed CO and adsorbed oxygen, E_3, has been found from several studies to be in the range 33–96 kJ/mol, although they contend that a value as low as 33 kJ/mol may not be justified. Several studies (22, 24, 41–43) have used values of 40–80 kJ/mol for E_3 to describe CO oxidation on platinum. The value of $E_3 = 74.5$ kJ/mol used in this study falls in the range of values from these other studies. Although the value of the activation energy for gaseous N_2O dissociation on Pt, E_2, is not readily available from prior experimental studies reported in the literature, values of 146 kJ/mol (33) and 75 kJ/mol (17) have been used in modelling studies for the activation energy of dissociation of adsorbed N_2O as compared with a value of $E_2 = 92$ kJ/mol used in this study.

As shown in Figs. 1–4, Mechanism 4 can provide an excellent description of the experimental observations. However, some caution must still be exercised because it is found that several quite dissimilar sets of parameter values can all produce similar descriptions of the data. This difficulty has previously been noticed by Graham and Lynch (22) and can only be resolved by using both dynamic and steady-state data when estimating parmeter values. Thus, while it is not possible to change an individual parameter value from that given in Table 2 without producing an increased model–experimental discrepancy, it nevertheless is possible to maintain excellent model–experimental agreement by making simultaneous adjustments to several (or all) of the parameter values. This is shown in Table 3, where three alternative sets of parameter values (Cases I–III) are given which produce very similar (essentially identical) model predictions compared to the base case parameters. As can be seen from Table 3, the low values of CO desorption energy, E_{-1}, and preexponential factor, k^0_{-1}, are consistent with the model

TABLE 3

Sets of Kinetic Parameters for Mechanism 4 which Give Similar Predictions

Parameter	Base case	Case I	Case II	Case III
K_1 (499 K)	1200	900	1100	960
K_{21} (499 K)	0.0173	0.012	0.0123	0.0128
K_{23} (499 K)	8	7.85	4	8
$K_{1,H}$ (499 K)	1.308×10^{-6}	1.3×10^{-6}	1.0×10^{-6}	1.27×10^{-6}
N_{CO}	1.025	1.02	1.0275	1.025
E_{-1}	41.0	49.8	39.7	51.0
E_2	92.0	79.1	85.8	78.7
E_3	74.5	65.7	75.3	65.7
k^0_{-1}	1.305×10^6	1.513×10^7	8.16×10^5	1.847×10^7
k^0_2	4.902×10^9	2.013×10^8	4.669×10^8	1.857×10^8
k^0_3	4.684×10^{11}	5.185×10^{10}	4.381×10^{11}	5.093×10^{10}
S_{CO}	0.01	0.01	0.01	0.01

prediction of the surface being saturated with CO in the low CO conversion region. The model predictions for the high CO conversion region (with low %CO in the feed) show that the fractional CO surface converge is less than 0.4.

To examine further the effect of the coverage dependence of the CO desorption activation energy on the model predictions, a step change in the CO adsorption and desorption rate constants was incorporated in the model. With this modification the CO conversion was calculated using the parameters listed in Table 2 while decreasing the feed %CO, and a step change in the values of E_{-1}, k^0_{-1}, and S_{CO} to 134 kJ/mol, 10^{15} s^{-1}, and 0.6, respectively, was made at the low-to-high bifurcation point. The predictions from the modified model are shown in Fig. 6. As can be seen from Fig. 6, the CO conversions in the high conversion region are in excellent agreement with the experimental data. However, because the parameters K_1 and K_{23} are coverage dependent, the rate expression is not explicit in terms of gas-phase concentrations of CO and N_2O.

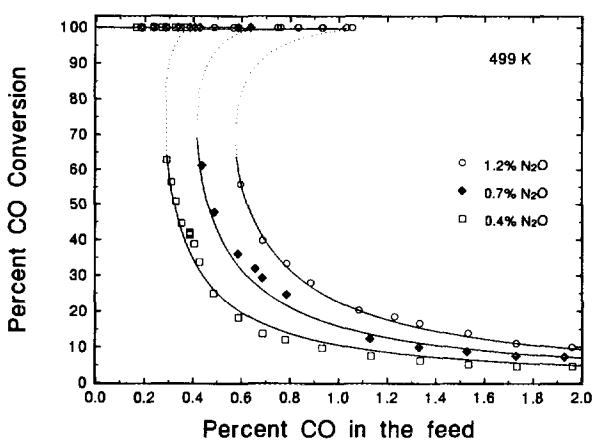

FIG. 6. Predictions from Mechanism 4 at 499 K with coverage-dependent CO adsorption and desorption rate constants.

Notwithstanding the concern with respect to uniqueness of the values of the model parameters, of the four mechanisms examined herein, Mechanism 4 incorporating the CO self-exclusion effect is the only kinetic model that predicts CO conversions for the low-conversion steady states which are as high as the values obtained experimentally. However, as seen in Fig. 1, in the region of high CO conversion a slight discrepancy is apparent between the model and the experimental data, particularly for very low values of %CO in the feed. As shown in Fig. 6, it is possible to predict CO conversions near 100% for low %CO in the feed by incorporating coverage dependent CO adsorption and desorption rate constants. It is also possible to predict CO conversions near 100% for low %CO in the feed by incorporating an oxygen self-exclusion effect in the model. Herz and Marin (44) have proposed the existence of such an effect in an attempt to describe the steady-state oxidation of CO by O_2 on supported platinum catalysts. In their model, the oxygen self-exclusion effect was very large, with oxygen being excluded from up to one-half of the surface ($N_O = 2$). Lynch (45) used a similar oxygen self-exclusion effect to describe CO oxidation on a Pt catalyst during forced composition cycling. Incorporation of this effect into Mechanism 4 (or Mechanism 1) would modify the balance equation for surface oxygen as follows:

$$k_2 L[N_2O](1 - \theta_{CO} - \theta_O)\frac{(1 - N_O\theta_O)}{(1 - \theta_O)} - k_3 L^2 \theta_O \theta_{CO} = 0. \quad [27]$$

However, if the oxygen self-exclusion effect is incorporated in Mechanism 4, it is not possible to obtain an explicit rate expression in terms of CO and N_2O concentrations. Therefore, the effect of oxygen self-exclusion was tested on Mechanism 1. From the solution of Eqs. [5], [10], [11], and [27] it is found that CO conversions of near 100% can be obtained for feed CO of less than 0.2% by using a very small value of $N_O = 1.008$ for the oxygen self-exclusion factor.

CONCLUSIONS

The N_2O + CO reaction over an alumina-supported platinum catalyst exhibits steady-state multiplicity in the temperature range 461–520 K. To our knowledge, this is the first report of steady-state multiplicity for the N_2O + CO reaction. The effects of temperature and feed composition on the bifurcation boundaries have been determined. The bifurcation points shift in the direction of increasing feed %CO with increasing temperature and with increasing $\%N_2O$ in the feed.

All of the four kinetic models examined in this study were able to predict the existence of steady-state multiplicity. However, for high values of %CO in the feed, only a model based on a CO self-exclusion effect could quantitatively both describe the bifurcation point locations as well as predict CO conversions which were in agreement with the experimental observations. The same conclusion has previously been reached by Graham and Lynch (22) from an examination of several possible mechanisms for the O_2 + CO reaction on a supported platinum catalyst. The proposed mechanism consists of several elementary steps, namely, the reversible adsorption of CO, the irreversible dissociative adsorption of N_2O to form gaseous N_2 and adsorbed atomic oxygen, and the surface reaction between adsorbed CO and adsorbed atomic oxygen to form gaseous CO_2. The CO self-exclusion effect allows N_2O to adsorb on a CO saturated surface and, therefore, the predicted CO conversions for high %CO in the feed are as high as the experimental values. Complete model–experimental agreement in the high-conversion region required either the incorporation of a coverage dependent CO desorption activation energy or the use of an oxygen self-exclusion effect.

APPENDIX: NOTATION

a	total surface area of supported catalyst, 9.4 m^2
$[CO]$	reactor CO concentration, mol/m^3
$[CO]_O$	feed CO concentration, mol/m^3
CO–M	adsorbed CO species on catalyst surface
C_S	gas-phase concentration of CO at catalyst particle surface, mol/cm^3
D_{eff}	effective diffusion coefficient for CO into an alumina pellet with a BET surface area of 109 m^2/g and an average pore size of 3 nm, 2.3×10^{-4} cm^2/s
E_{LH}/R	slope of Arrhenius-type curve for model parameter K_{LH}, K
E_1/R	slope of Arrhenius-type curve for model parameter K_1, K
E_{-1}	activation energy for CO desorption, kJ/mol
E_2	activation energy for N_2O dissociation, kJ/mol
E_3	activation energy for surface reaction, kJ/mol
E_{21}/R	slope of Arrhenius-type curve for model parameter K_{21}, K
E_{23}/R	slope of Arrhenius-type curve for model parameter K_{23}, K
k_1	CO adsorption rate constant, $6.87\ S_{CO}\sqrt{T}/L$, $m^3/mol \cdot s$
k_{-1}	Co desorption rate constant, $k^0_{-1} \exp(-E_{-1}/RT)$, s^{-1}
k^0_{-1}	CO desorption preexponential factor, s^{-1}
k_2	N_2O dissociation rate constant, $k^0_2 \exp(-E_2/RT)$, $m^3/mol \cdot s$
k^0_2	N_2O dissociation preexponential factor, $m^3/mol \cdot s$
k_3	surface reaction rate constant, $k^0_3 \exp(-E_3/RT)$, $m^2/mol \cdot s$
k^0_3	surface reaction preexponential factor, $m^2/mol \cdot s$
k_4	Eley–Rideal reaction rate constant, $m^3/mol \cdot s$
k_5	N_2O adsorption rate constant, $m^3/mol \cdot s$
k_{-5}	N_2O desorption rate constant, s^{-1}
k_6	N_2O–M dissociation rate constant, s^{-1}
K_1	ratio of CO adsorption to desorption rate constants, (k_1/k_{-1}), m^3/mol
K_{21}	ratio of N_2O decomposition to CO desorption rate constants, (k_2/k_{-1}), m^3/mol
K_{23}	ratio of N_2O decomposition to surface reaction rate constants, (k_2/k_3L), m^3/mol
K_{31}	ratio of surface reaction to CO desorption rate constants, (k_3L/k_{-1})
K_{43}	ratio of Eley–Rideal to surface reaction rate constants, (k_4/k_3L), m^3/mol
K_5	ratio of N_2O adsorption to desorption rate constants, (k_5/k_{-5}), m^3/mol
K_{63}	ratio of N_2O–M decomposition to surface reaction rate constants, (k_6/k_3L), m^3/mol
K_{65}	ratio of N_2O–M decomposition to N_2O desorption rate constants, (k_6/k_{-5})
K_{LH}	surface reaction rate parameter, (ak_3L^2/W), $mol/g \cdot s$
L	adsorption capacity of platinum surface, 2×10^{-5} mol/m^2
M	vacant site on platinum surface
N_{CO}	CO self-exclusion factor
N_O	oxygen self-exclusion factor
$[N_2O]$	reactor N_2O concentration, mol/m^3
$[N_2O]_O$	feed N_2O concentration, mol/m^3
N_2O–M	adsorbed N_2O species on catalyst surface
O–M	adsorbed oxygen species on catalyst surface
Q	total feed flow rate to the reactor at reactor conditions, $1.11 \times 10^{-8}\ T$, m^3/s
$-R_{CO}$	observed reaction rate based on catalyst volume, $mol/s \cdot cm^3$
$\mathbf{r}_{CO,ads}$	rate of CO adsorption, $mol/m^2 \cdot s$
$\mathbf{r}_{CO_2}$	rate of CO_2 formation, $mol/g \cdot s$
r_p	radius of catalyst particle, (3 × volume/surface area), 0.015 cm
S_{CO}	CO sticking probability on platinum catalyst surface
T	reactor temperature, K
W	mass of catalyst, 20 g

Greek Letters

θ_{CO}	fractional CO surface coverage
θ_{N_2O}	fractional N_2O surface coverage

θ_O fractional oxygen surface coverage
Φ_S Thiele modulus

ACKNOWLEDGMENT

This work has been supported by the Natural Sciences and Engineering Research Council of Canada.

REFERENCES

1. Bolten, H., Hahn, T., LeRoux, J., and Lintz, H. G., *Surf. Sci.* **160,** L529 (1985).
2. Schwartz, S. B. and Schmidt, L. D., *Surf. Sci.* **206,** 169 (1988).
3. Adlhoch, W. and Lintz, H. G., *Z. Phys. Chem. N. F.* **103,** 207 (1976).
4. Adlhoch, W., Lintz, H. G., and Weisker, T., *Surf. Sci.* **103,** 576 (1981).
5. Lesley, M. W. and Schmidt, L. D., *Surf. Sci.* **155,** 215 (1985).
6. Schwartz, S. B. and Schmidt, L. D., *Surf. Sci.* **183,** L269 (1987).
7. Schüth, F. and Wicke, E., *in* "Instationary Processes and Dynamic Experimental Methods in Catalysis, Electrochemistry and Corrosion" (G. Sandstede and G. Kreysa, Eds.), Dechema Monogr., Vol. 120, p. 429. Dechema, Frankfurt-am-Main, 1989.
8. Imbihl, R., Fink, Th., and Krisher, K., *J. Chem. Phys.* **96,** 6236 (1992).
9. Shelef, M. and Otto, K., *J. Catal.* **10,** 408 (1968).
10. Lambert, R. M. and Comrie, C. M., *Surf. Sci.* **46,** 61 (1974).
11. Adlhoch, W. and Lintz, H. G., *Surf. Sci.* **78,** 58 (1978).
12. Lorimer, D. and Bell, A. T., *J. Catal.* **59,** 223 (1979).
13. Hecker, W. C. and Bell, A. T., *J. Catal.* **84,** 200 (1983).
14. Klein, R. L., Schwartz, S., and Schmidt, L. D., *J. Phys. Chem.* **89,** 4908 (1985).
15. Lim, K. J., Löffler, D. G., and Boudart, M., *J. Catal.* **100,** 158 (1986).
16. Cho, B. K., Shanks, B. H., and Bailey, J. E., *J. Catal.* **115,** 486 (1989).
17. McCabe, R. W. and Wong, C., *J. Catal.* **121,** 422 (1990).
18. Kudo, A., Steinberg, M., Bard, A. J., Campion, A., Fox, M. A., Malloux, T. E., Webber, S. E., and White, J. M., *J. Catal.* **125,** 565 (1990).
19. Adlhoch, W., Kohler, R., and Lintz, H. G., *Z. Phys. Chem. N. F.* **120,** 111 (1980).
20. Lintz, H. G., *Surf. Sci.* **108,** L486 (1981).
21. Cho, B. K., *J. Catal.* **138,** 255 (1992).
22. Graham, W. R. C. and Lynch, D. T., *AIChE J.* **33,** 792 (1987).
23. Lynch, D. T. and Wanke, S. E., *J. Catal.* **88,** 333 (1984).
24. Graham, W. R. C. and Lynch, D. T., *AIChE J.* **36,** 1796 (1990).
25. Lynch, D. T. and Walters, N. P., *Chem. Eng. Sci.* **45,** 1089 (1990).
26. Matsuura, T. and Kato, M., *Chem. Eng. Sci.* **22,** 171 (1967).
27. Eigenberger, G., *Chem. Eng. Sci.* **33,** 1255 (1978).
28. Satterfield, C. N., "Heterogeneous Catalysis in Practice," p. 349. McGraw–Hill, New York, 1980.
29. Smith, T. G., Zahradnik, J., and Carberry, J. J., *Chem. Eng. Sci.* **30,** 763 (1975).
30. Engel, T. and Ertl, G., *Adv. Catal.* **28,** 1 (1979).
31. Lintz, H. G. and Riekert, L., *J. Catal.* **88,** 244 (1984).
32. Alnot, M., Cassuto, A., Fusy, J., and Pentenero, A., *Jpn. J. Appl. Phys. Suppl.* **2**(2), 79 (1974).
33. Takoudis, C. G. and Schmidt, L. D., *J. Catal.* **80,** 274 (1983).
34. Schmidt, L. D., Hansenberg, D., Schwartz, S., and Papapolymerou, G. A., *in* "Catalyst Characterization Science—Surface and Solid State Chemistry" (M. L. Deviney and J. L. Gland, Eds.), ACS Symposium Series 288, p. 177. Am. Chem. Soc., Washington, DC, 1985.
35. The Math Works Inc., "The Student Edition of MATLAB—For MS-DOS Personal Computers," p. 394. Prentice–Hall, Englewood Cliffs, NJ, 1992.
36. Freel, J., *J. Catal.* **25,** 149 (1972).
37. Dorling, T. A. and Moss, R. L., *J. Catal.* **7,** 378 (1967).
38. Yao, H. C., Sieg, M., and Plummer, H. K., *J. Catal.* **59,** 365 (1979).
39. Ertl, G., Neumann, M., and Streit, K. M., *Surf. Sci.* **64,** 393 (1977).
40. Seebauer, E. G., Kong, A. C. F., and Schmidt, L. D., *Surf. Sci.* **176,** 134 (1986).
41. Lynch, D. T., Emig, G., and Wanke, S. E., *J. Catal.* **97,** 456 (1986).
42. Kurtanjek, Ž. and Froment, G. F., *Chem. Eng. Sci.* **40,** 3189 (1991).
43. Sales, B. C., Turner, J. E., and Maple, M. B., *Surf. Sci.* **114,** 381 (1982).
44. Herz, R. K. and Marin, S. P., *J. Catal.* **65,** 281 (1980).
45. Lynch, D. T., *Can. J. Chem. Eng.* **62,** 601 (1984).